A Virtual MRI Scanner for Simulating Arbitrary Pulse Sequences on High-Resolution Virtual Phantoms

J. Magland[1], B. Vasilic[1], F. W. Wehrli[1]

[1]Laboratory for Structural NMR Imaging, Department of Radiology, University of Pennsylvania Medical Center, Philadelphia, PA, United States

Introduction

Numerical simulations of the Bloch equation have been used by NMR researchers for optimizing pulse sequences, interpreting NMR measurements, analyzing artifacts, and validating experimental results. The nature of these simulations varies widely. One approach is to represent the object (virtual phantom) as a large collection of spins or isochromats, and numerically solve the Bloch equation one particle at a time throughout the pulse sequence [1]. Another approach is to compute basis images (e.g. from actual in vivo images), representing T1, T2 and proton density on a pixel-by-pixel basis and then use analytical formulas for the signal intensity based on sequence-dependent spin-dynamics [2]. The first approach becomes infeasible for high-resolution 3D virtual phantoms since the execution time is proportional to the number of phantom particles as well as the pulse sequence length (or complexity). The second approach is computationally trivial but limited to pulse sequences which have analytical signal equations. A third technique is to decompose the virtual phantom into tissue types (as above), and then use a numerical simulation for each tissue [3]. This approach produces realistic images for certain pulse sequences under ideal circu mstances. Although partial volume and other effects can be incorporated into these simulations, none of these methods can fully simulate the range of MRI artifacts and phenomena predicted by the Bloch equation for arbitrary pulse sequences.

An efficient MRI simulator is described for use with user-specified pulse sequences and high-resolution 3D virtual phantoms. The simulator models T1, T2, and T2* relaxation as well as arbitrary spectral composition. Phenomena predicted by the Bloch equation are accurately represented. For example, artifacts caused by chemical shift, approach to steady-state, off-resonance, or an imperfect B_1 field, as well as the effects of finite sampling (e.g. Gibbs ringing), stimulated echo artifacts and partial volume effects are all handled automatically.

Methods

At each time point during the sequence, the magnetization of each tissue type is modeled as a sum of (possibly thousands of) transverse and longitudinal components. Each component is a pair consisting of a complex weight along with a point in 4-dimensional k-space (3 spatial frequency plus time). The different components represent coherence pathways that the magnetization follows during the MR experiment. A hard (instantaneous) RF pulse splits each term into 3 terms (1 longitudinal and 2 transverse), while applied gradients simply shift the terms in k-space. As the terms evolve with T1 and T2 relaxation, they become negligible and are dropped according to a preset threshold. When a readout event is encountered, the transverse terms are all evaluated on the virtual k-space which is the preloaded Fourier transform of a large 3D spin-density array. This evaluation also takes into consideration T2* and spectral information. These values are summed to generate the raw data, as though it had come from a true MR scanner (see **Figure 1**).

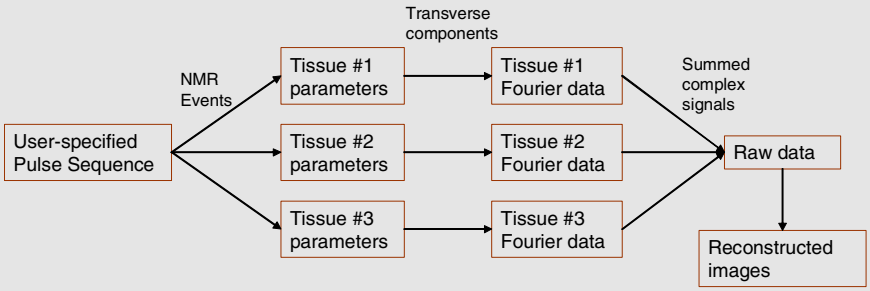

Figure 1: Overview of the simulator. Tissue parameters such as T1 and T2 are combined with NMR events to produce a collection of transverse magnetization terms. At a point during the sequence, the number of such terms is typically in the thousands. For each readout event, these terms are evaluated on the spin-density Fourier data (which has been loaded into memory) and the results are summed against complex weights to generate the raw data file. The raw data is processed exactly as if it had come from a true MR scanner.

Results and Discussion

Figure 2 shows images reconstructed using the raw data produced by the MRI simulator (see caption for details). Each scan took less than one minute on a Pentium IV, 3.06 GHz PC. The simulator works best with non-selective pulses, although selective pulses can also be used with a significant penalty in efficiency. An alternative in most cases is to modify the virtual phantom to reflect the slice selection. Background field inhomogeneity can be incorporated with a penalty in computing efficiency unless the inhomogeneity is linear across the field-of-view (see **Figure 2c**).

In theory the execution time is independent of the data size of the virtual phantom's spin-density array. This opens the possibility of performing realistic MR simulations on very high resolution virtual phantoms, such as segmented micro-CT data sets. Furthermore, the simulator provides a realistic framework for debugging and optimizing novel pulse sequences.

Figure 2: Images of virtual phantoms reconstructed using the raw data generated by the MRI simulator. In (a), (b), and (c), the virtual phantom consisted of two tissue types simulating edible oil (to mimic adipose tissue) and doped water. The spin-density array was 1500x1100x6 voxels. The following parameters were used:
water: T1=600ms, T2=200ms
oil: T1=300ms, T2=40ms.
The spectrum of the oil was created to match the literature [4].
For (d), the McGill Univ. standard brain model [5] was used (CSF, white and grey matter only). The spin-density array for the brain was resampled to 500x500x50 voxels.

(a) Fast 2D spin-echo, TR=80 ms, 256 PE steps.
Execution time = 13 sec.
Approx. 4,000 terms

(b) 2D Projection reconstruction, TR = 200 ms, 720 views, 256x256 matrix.
Execution time = 9 sec.
Approx. 200 terms.

(c) 2D SSFP, TR=50 ms, 256x256 linear background inhomogenity: 40 Hz across the FOV.
Execution time = 5 sec.
Approx. 2,000 terms.

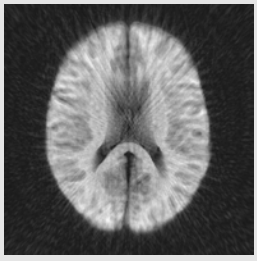

(d) Undersampled 3D Projection reconstruction (PE in 3rd direction), TR = 200 ms, 90 views, 256x256x16 recon.
Execution time = 45 sec.
Approx. 2,000 terms.

References:
[1] Summers et al, Magn Reson Med 3 (1986).
[2] Bobman et al, Radiol 155 (1985).
[3] Kwan et al, IEEE Trans Med Imag 18 (1999).
[4] Hilaire et al. Magn Reson Imag 18 (2000).
[5] http://www.bic.mni.mcgill.ca/brainweb/

Acknowledgement: NIH Grant T32 EB000814